Radiation Protection Dosimetry, 2026, **202(18)**, 1552–1564
https://doi.org/10.1093/rpd/ncag089
Published: 18 August 2026
Paper

OXFORD

Environmental monitoring of static magnetic fields around operating high-voltage direct-current transmission facilities in Japan

Fumiaki Kawabe*, Shinichi Muroya, Chiyoji Ohkubo

Japan EMF Information Center, 2-9-11 Shiba, Minato-ku, Tokyo 105-0014, Japan
*Corresponding author. Japan EMF Information Center, 2-9-11 Shiba, Minato-ku, Tokyo 105-0014, Japan. E-mail: Kawabe_f@jet.or.jp

Abstract

Static magnetic fields are present around high-voltage direct-current transmission facilities, but on-land environmental measurement data under actual operating conditions remain limited. This study measured three-axis magnetic flux densities at 1.0 m above ground at 38 accessible locations around all four operating direct-current transmission links in Japan, including overhead-line and underground-cable sections. Resultant magnetic flux densities ranged from 39.7 to 154.8 μT, while measured local geomagnetic-field levels ranged from 46.6 to 50.6 μT. The maximum value was observed above the Anan-Kihoku Link underground-cable section and was far below the International Commission on Non-Ionizing Radiation Protection (ICNIRP) reference level for general public exposure to static magnetic fields. Lateral-profile measurements showed that values near the lines or cable routes diminished to local geomagnetic-field levels within several tens of metres. Geomagnetic-field-aware calculations were generally consistent with representative measured profiles, although underground-cable comparisons were sensitive to cable-centreline uncertainty. These data support static magnetic-field exposure assessment around operating direct-current transmission facilities.

Introduction

In recent years, the large-scale deployment of renewable energy sources, such as wind power generation and photovoltaic systems, has driven the construction of long-distance transmission lines that interconnect power systems between countries and regions. In Japan as well, new construction and capacity expansion projects of high-voltage direct-current transmission lines have been carried out to enhance the interregional interconnection capacity between the eastern and western power systems. Currently, four direct-current transmission lines are in operation in Japan. Furthermore, according to the "Wide-Area Grid Long-Term Policy" published by the Organization for Cross-regional Coordination of Transmission Operators, Japan (OCCTO) [1], additional direct-current interconnection projects are planned in the future.

The Japan EMF Information Center (JEIC) has served as a risk communication centre regarding electromagnetic fields (EMF). As part of risk communication activities, JEIC also measures magnetic flux density generated by electrical power facilities and household appliances and publicly discloses the results. To date, public inquiries related to EMF generated by power facilities such as alternating-current transmission lines have continued, and public interest in magnetic fields generated by direct-current transmission lines is also expected to increase as direct-current facilities expand.

For context, static magnetic fields are also encountered in daily environments. As shown in the Geomagnetic Chart of Japan for the epoch 2020.0 [2], the total intensity of the geomagnetic field over the main islands of Japan is ∼50 μT. In a previous measurement study by JEIC, module-generated static magnetic fields from

Received: 1 June 2026. **Revised:** 18 July 2026. **Accepted:** 22 July 2026
© The Author(s) 2026. Published by Oxford University Press.
This is an Open Access article distributed under the terms of the Creative Commons Attribution-NonCommercial License (https://creativecommons.org/licenses/by-nc/4.0/), which permits non-commercial re-use, distribution, and reproduction in any medium, provided the original work is properly cited. For commercial re-use, please contact reprints@oup.com for reprints and translation rights for reprints. All other permissions can be obtained through our RightsLink service via the Permissions link on the article page on our site—for further information please contact journals.permissions@oup.com.

photovoltaic modules, estimated after subtracting the local geomagnetic-field components, were 1.70–11.1 μT at a distance of 0.20 m from the modules under maximum output-current conditions [3]. These module-generated values were lower than the typical geomagnetic-field level in Japan. This comparison is useful when interpreting static magnetic-field measurements around direct-current transmission facilities because the measured resultant field includes both the facility-related magnetic field and the local geomagnetic field.

Many previous studies on direct-current transmission lines have focused on their effects on plants and other organisms [4] or on marine organisms [5]. In particular, numerous investigations have examined the impacts on marine species such as crabs [6, 7], lobsters [8], and sharks [5], including magnetic field exposure experiments. With respect to magnetic field measurements and simulations, several studies have reported magnetic field simulations for submarine cables [9–11] and have evaluated magnetic field levels and lateral field characteristics. However, measured magnetic field data around overhead and underground direct-current transmission lines on land [12, 13] have been relatively limited. For overhead direct-current lines, some studies have addressed ion currents and electric fields [4] and a limited number of magnetic field measurement cases in Japan [14] have been reported, whereas field measurements specifically focusing on magnetic fields remain scarce [15].

Assessment of static magnetic fields around direct-current facilities is also methodologically different from conventional alternating-current magnetic field evaluation. In alternating-current assessments, the geomagnetic field is typically not a major issue. In contrast, static magnetic field measurements around direct-current transmission lines include the contribution of the geomagnetic field and therefore require explicit treatment of vector components and sensor orientation relative to the line direction or cable-route direction. This point is important when interpreting measured resultant magnetic flux densities and lateral field profiles around direct-current facilities.

Against this backdrop, this study provides environmental monitoring data on static magnetic fields in the vicinity of operating high-voltage direct-current transmission facilities under actual operating conditions. The study had three objectives. First, three-axis magnetic flux densities were measured at accessible on-land locations covering both overhead-line and underground-cable sections for all four operating direct-current transmission links in Japan. Second, the measured resultant magnetic flux densities were evaluated in relation to local geomagnetic field levels and the ICNIRP reference level for general public exposure to static magnetic fields. Third, representative lateral profiles were examined to characterize the spatial decrease in magnetic flux density with distance from transmission lines or cable routes and to identify the distances at which the measured fields diminished to local geomagnetic-field levels under the investigated conditions. Geomagnetic-field-aware calculations were performed for selected representative profiles where line-specific current and geometric information were available, and the details are provided in the Supplementary Material.

The results of this study are intended to support environmental monitoring, exposure assessment, and communication of static magnetic-field exposure levels associated with direct-current transmission systems.

Overview of high-voltage direct-current transmission lines in Japan

Figure 1 shows the locations of the four operating and two planned direct-current transmission lines in Japan. Table 1 summarizes the main characteristics of the four operating direct-current transmission lines. Currently, four direct-current transmission lines are in operation in Japan: the Kitahon Link (hereafter referred to as “KH” Link) and the Hokuto–Imabetsu Link (hereafter referred to as “HI” Link), which interconnect Hokkaido and Aomori Prefecture; the Hida–Shinano Link (hereafter referred to as “HS” Link), which interconnects Gifu and Nagano Prefectures; and the Anan–Kihoku Link (hereafter referred to as “AK” Link), which interconnects Tokushima and Wakayama Prefectures.

The KH Link [16] was constructed as the first interconnection facility between Hokkaido and Honshu and began operation in 1979. It is a bipolar single-circuit direct-current transmission line rated at $\pm$250 kV, 1200 A, and 600 MW. The link comprises 124 km of overhead transmission lines and 43 km of underground cables. The HI Link [17] was constructed as a second direct-current interconnection between Hokkaido and Honshu, in addition to the KH Link, to increase the transmission capacity between the two islands. It commenced operation in 2019. This link is a monopolar single-circuit direct-current transmission line rated at 250 kV, 1200 A, and 300 MW and comprises 98 km of overhead transmission lines and 24 km of underground cables. The HS Link [18, 19] was constructed as a direct-current interconnection between the 60 and 50 Hz power system areas in Japan. It began operation in 2021. The link is a bipolar single-circuit direct-current transmission line rated at $\pm$200 kV, 2250 A, and 900 MW and comprises 90 km of overhead transmission line. The AK Link (Kii Channel Link) [20] was constructed as a direct-current interconnection

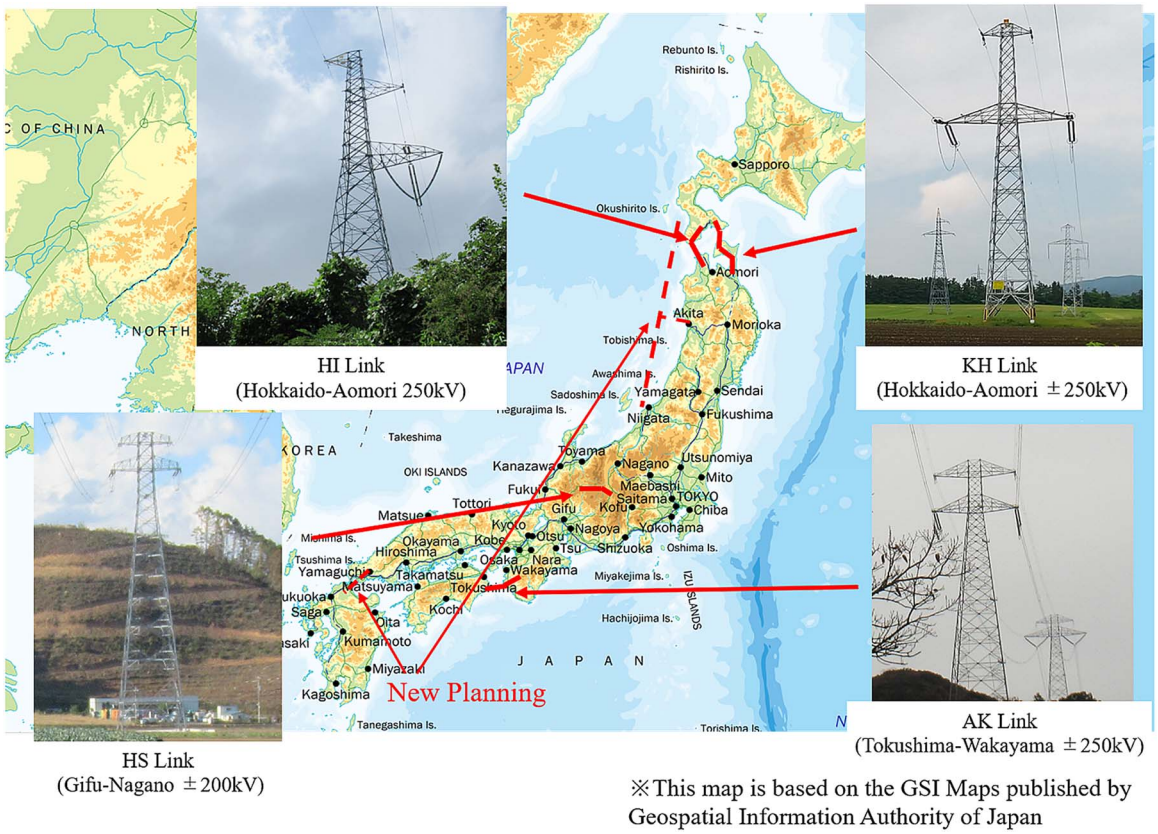


Figure 1 Locations of direct-current transmission lines in Japan.

Table 1 Main characteristics of four operating direct-current links in Japan.

Transmission line	Voltage	Rated current / Capacity	Commissioned	Length (Overhead)	Length (Cables)
KH Link	±250 kV	1200 A / 600 MW	1979	124 km	43 km
HI Link	250 kV	1200 A / 300 MW	2019	98 km	24 km
HS Link	±200 kV	2250 A / 900 MW	2021	90 km	-
AK Link	±250 kV	2800 A / 1400 MW	2000	51 km	49 km

between Honshu and Shikoku. It began operation in 2000. The link is a bipolar single-circuit direct-current transmission line rated at ±250 kV, 2800 A, and 1400 MW and comprises 51 km of overhead transmission lines and 49 km of underground cables. According to the "Wide-Area Grid Long-Term Policy" published by OCCTO in 2023, construction projects for two additional direct-current links, one between Hokkaido, Tohoku, and Tokyo and another between Chugoku and Kyushu are planned to facilitate the effective utilization of renewable energy resources in regions such as Hokkaido and Kyushu. In particular, the planned Hokkaido–Tohoku–Tokyo high-voltage direct-current project is a large-scale system with a total length of ~1000 km and a transmission capacity of 4000 MW.

Materials and methods

Measurement instrument

Static magnetic fields were measured using a periodically calibrated fluxgate-type magnetometer capable

Table 2 Main specifications of the magnetometer.

Item	Specification
Detection principle	Parallel fluxgate method
Effective measurement range	100.0 μT / 1000.0 μT
Minimum resolution	0.01 μT / 0.1 μT
Frequency range	DC to 200 Hz; step response ($\pm$100.0 μT): approx. 0.8 ms in DC mode
Linearity (direct-current magnetic field)	Error within $\pm$0.5% of F.S.
Operating conditions	Temperature 0–40 °C; humidity $\leq$85%
Main unit dimensions	350 mm (W) $\times$ 132 mm (H) $\times$ 300 mm (D)
Main unit mass	Approx. 5 kg

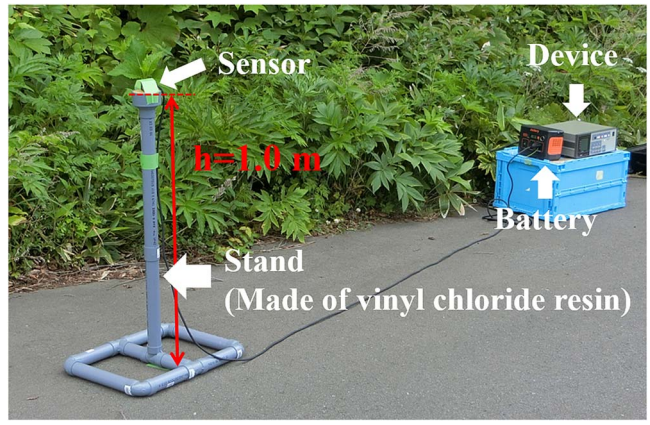


Figure 2 Overview of the measurement instrument, including the magnetometer (MTI FM-3400A).

of measuring along three orthogonal axes (FM-3400A, MTI Co., Ltd.). The instrument was used in accordance with the relevant requirements of IEC 61786–1:2013 [21] under the environmental conditions of this study. The FM-3400A offers measurement ranges of 100 and 1000 μT, with corresponding resolutions of 0.01 and 0.1 μT, respectively. The measurement error is $\pm$0.5% of full scale (F.S.) for each axis. The magnetometer consists of a sensor, a probe, a monitor, a battery, and a main unit with embedded measurement and control circuits. The monitor displays the measured values, which are sampled continuously at intervals of $\sim$0.8 s. The main specifications of the magnetometer are shown in Table 2. Although the specified operating temperature range of the instrument is 0°C–40°C, all field measurements in this study were conducted within this range. Figure 2 shows an overview of the measurement instrument.

Field measurement procedure

Measurements were conducted at a height of 1.0 m above ground level in accordance with IEC 61786–2:2014 [22], which specifies measurement procedures for human exposure. For measurements around direct-current electric power systems, IEC 61786–2 refers to relevant measurement procedures specified in IEC 62110:2009 [23], which was developed for field measurements around alternating-current power systems. According to those procedures, magnetic fields under overhead transmission lines are measured at a height of 1.0 m above ground level, whereas magnetic fields above underground cables are generally measured at three heights: 0.5, 1.0, and 1.5 m above ground level. However, IEC 61786–2 also allows measurements above direct-current underground cables to be conducted at a height of 1.0 m when the magnetic field is considered to be sufficiently uniform above the cables. Therefore, a measurement height of 1.0 m was adopted uniformly at all measurement points, for both overhead lines and underground cables, to provide a consistent basis for environmental monitoring and comparison among measurement locations.

Initially, a carbon-fiber tripod was used as a mounting fixture for the sensor. However, the tripod affected

the measured static magnetic field around the sensor, resulting in unstable measurement values. Therefore, as shown in Fig. 2, a custom-made mounting fixture constructed from polyvinyl chloride (PVC) pipe was used for all measurements.

The sensor was fixed at a height of 1.0 m using the PVC fixture. During measurement, the sensor y-axis was aligned with the transmission-line or cable-route direction. For the KH Link, HI Link and HS Link, the measurement range of the magnetometer was set to 100.0 μT, whereas for the AK Link it was set to 1000.0 μT because some measured values exceeded 100 μT.

Since measurements of static magnetic fields can be affected by nearby metallic objects, such as conductive tripods, transmission towers, distribution lines, guardrails, fences, and reinforced concrete retaining walls, measurement sites were selected to minimize the influence of surrounding metallic structures.

From the perspective of public exposure assessment, measurement locations were selected in areas accessible to the general public. Furthermore, for overhead transmission lines, measurement points were selected so that the distance between the conductors and the measurement location was minimized, thereby enabling the evaluation of magnetic flux density levels near the conductors. Measurements for overhead transmission lines were conducted at the midpoint between the conductors. For underground cable sections, measurements were conducted above the nominal cable route at a height of 1.0 m above ground level.

At each measurement point, after the displayed values had stabilized, the three orthogonal magnetic flux density components (x, y, and z) and the resultant magnetic flux density were recorded. A total of 38 measurement points were selected across the four direct-current transmission systems investigated in this study. Among the four direct-current transmission systems, HS Link and AK Link had periods during which the transmitted power remained nearly constant and current fluctuations were minimal. During these periods, the magnetic field values were stable, and the stabilized values were recorded. In addition, measurements of the horizontal distance dependence of the magnetic field were performed for these systems. For the KH Link and HI Link, the current values fluctuated depending on power demand between different regions. When the displayed values were unstable, the maximum stabilized value observed during the measurement period, typically several minutes, was recorded as a conservative point value for exposure-level assessment. The values reported in this study should therefore be interpreted as stabilized point readings, or maximum stabilized readings when the displayed values fluctuated during the measurement period, under the operating conditions at the time of measurement. They are not long-term time-weighted averages.

OCCTO publishes power flow data for direct-current transmission systems at 30-minute intervals for the HS Link and 5-minute intervals for the AK Link. For the HS Link and AK Link, line-specific current values during magnetic-field measurements were derived from these data and used for the representative measurement–calculation comparisons. For the KH Link and HI Link, only aggregated power-flow data were publicly available, and therefore individual line-specific current values could not be derived.

For overhead transmission lines, conductor heights above ground level were measured using a laser distance meter during the magnetic-field measurements. For underground cables, burial depths were obtained from engineering drawings.

Measurement of the background geomagnetic field

The magnetic flux density measured at each point includes the contribution of the geomagnetic field. To evaluate this contribution, the magnetic flux density at a height of 1.0 m above ground level was also measured at locations sufficiently distant from the direct-current transmission lines and, as far as practicable, free from nearby metallic objects. The measured values at these locations were considered representative of the local geomagnetic field. However, at some measurement points, no suitable nearby locations were available for geomagnetic field measurements because of terrain constraints, surrounding facilities, or limited accessibility. In such cases, local geomagnetic field measurements were not conducted.

Results

Overall measurement results

The measurement results for overhead transmission lines are shown in Table 3, and those for underground cables are shown in Table 4. The measured resultant static magnetic flux density, including the geomagnetic field contribution, ranged from 39.7 to 154.8 μT across the 38 measurement locations. The highest value, 154.8 μT, was observed in the underground-cable section of the AK Link under the operating conditions on the measurement day. The measured geomagnetic field values at locations

Table 3 Measurement results for overhead transmission lines.

Line	Section (Span between towers)	Date	Time	Conductor height above ground (m)	MFD (μT)	GMF (μT)
KH Link	No. 31–No. 32	2023/8/31	8:50	16.5	52.3	—
KH Link	No. 79–No. 80	2023/8/31	10:05	15.9	51.3	—
KH Link	No. 61–No. 62	2023/8/31	12:00	16.0	52.1	49.5
KH Link	No. 16–No. 17	2023/8/31	14:15	22.3	52.8	50.4
KH Link	No. 16–No. 17	2023/9/1	10:12	22.3	51.9	50.4
KH Link	No. 352–No. 353	2023/9/12	9:40	16.1	51.8	49.1
KH Link	No. 309–No. 310	2023/9/12	10:36	21.2	51.2	—
KH Link	No. 305–No. 306	2023/9/12	10:50	17.0	52.0	—
KH Link	No. 294–No. 295	2023/9/12	11:11	15.5	52.7	49.2
KH Link	No. 192–No. 193	2023/9/12	12:30	21.2	50.8	48.9
KH Link	No. 193–No. 194	2023/9/12	13:00	16.6	51.5	—
KH Link	No. 294–No. 295	2023/9/13	13:02	15.5	54.2	—
HI Link	No. 204–No. 205	2023/8/30	10:53	28.0	48.3	49.0
HI Link	No. 203–No. 204	2023/8/30	11:38	27.9	48.4	49.0
HI Link	No. 202–No. 203	2023/8/30	12:16	47.0	50.6	49.0
HI Link	No. 38–No. 39	2023/8/30	15:20	53.6	50.1	—
HI Link	No. 208–No. 208–1	2023/9/11	14:03	21.8	48.8	49.5
HI Link	No. 241–No. 242	2023/9/11	15:11	34.6	50.1	—
HI Link	No. 268–C/S	2023/9/11	15:50	22.7	49.0	—
HS Link	No. 69–No. 70	2023/10/25	13:45	51.6	48.9	46.6
HS Link	No. 69–No. 70	2023/10/25	14:07	37.3	50.8	46.6
HS Link	No. 37–No. 38	2023/10/26	9:50	37.0	50.7	46.6
HS Link	No. 194–No. 195	2023/10/26	14:40	19.5	59.4	46.6
HS Link	No. 195–No. 196	2023/10/26	15:54	21.9	47.5	46.6
HS Link	No. 196–No. 197	2023/10/26	9:12	22.1	52.2	47.8
HS Link	No. 196–No. 197	2024/4/25	12:20	22.2	56.6	47.8
HS Link	No. 194–No. 195	2024/4/25	13:50	19.3	59.9	46.6
AK Link	No. 7–No. 8	2023/12/12	8:57	64.5	49.3	46.8
AK Link	No. 10–No. 11	2023/12/12	9:20	102.4	47.8	47.9
AK Link	No. 10–No. 11	2024/5/30	14:00	102.8	48.1	47.9
AK Link	No. 8–No. 9	2024/5/30	9:50	65.2	49.6	46.8

Notes: MFD, measured resultant magnetic flux density at the measurement point, including the contribution of the geomagnetic field; GMF, geomagnetic field measured at a location sufficiently distant from the direct-current transmission line or cable route; C/S, converter station, where alternating-current power is converted to direct-current power

sufficiently distant from the transmission lines ranged from 46.6 to 50.6 μT.

The measured resultant magnetic flux density includes both the local geomagnetic field and the magnetic field generated by the direct-current transmission facility. Because magnetic flux density is a vector quantity, the facility-related field does not simply add to the geomagnetic field as a scalar value. Depending on the relative direction of the two fields, the resultant value may be either higher or lower than the local geomagnetic-field level. This explains why some measured values in the lateral profiles were lower than the measured local geomagnetic-field level.

Overhead-line and underground-cable measurements

The maximum measured value for overhead-line sections was 59.9 μT. At many overhead-line sites, accessible measurement locations were associated with relatively large conductor heights above ground. As a result, the direct-current-related magnetic-field contribution was

Table 4 Measurement results for underground cables.

Line	Section	Date	Time	Underground cable burial depth (m)	MFD (μT)	GMF (μT)
KH Link	Furukawa C/H–Landing Point	2023/8/31	10:00	1.1	45.1	50.6
KH Link	Furukawa C/H–Landing Point	2023/8/31	10:20	1.4	56.1	50.6
KH Link	Furukawa C/H–Landing Point	2023/8/31	10:32	0.8	56.4	50.6
KH Link	Landing Point–Sai C/H	2023/9/12	15:30	1.4	58.3	49.5
KH Link	Landing Point–Sai C/H	2023/9/12	15:50	1.1	65.8	49.5
KH Link	Landing Point–Sai C/H	2023/9/12	16:30	1.2	58.3	49.5
KH Link	Landing Point–Sai C/H	2023/9/13	10:15	1.2	47.8	49.5
HI Link	Yoshioka C/H–Landing Point	2023/8/30	10:53	2.3	39.7	49.0
HI Link	Landing Point–Tappi C/H	2023/9/11	13:26	2.1	44.8	49.5
HI Link	Landing Point–Tappi C/H	2023/9/11	13:30	2.1	45.4	49.5
AK Link	Underground section near Yura Switching station	2023/12/12	11:00	3.0	154.8	46.8
AK Link	Underground section near Yura Switching station	2024/5/30	10:00	2.5	121.1	46.8

Notes: MFD, measured resultant magnetic flux density at the measurement point, including the contribution of the geomagnetic field; GMF, geomagnetic field measured at a location sufficiently distant from the direct-current transmission line or cable route; C/H, cable head, a facility where underground cables are connected to overhead transmission lines.

small compared with the geomagnetic-field level at these locations. In contrast, underground-cable measurements generally involved shorter sensor-to-conductor distances because the measurements were conducted above the nominal cable route. Among the underground-cable measurements, the AK Link showed the highest values, 121.1–154.8 μT, even though its cable burial depth, 2.5–3.0 m, was slightly greater than those of the KH Link and HI Link, which ranged from 0.8 to 2.3 m. This difference is considered to be mainly associated with the substantially larger operating current of the AK Link. On the measurement days, the AK Link carried a total current of up to $\sim$5600 A. In contrast, the aggregated power-flow data for the KH Link and HI Link indicated much smaller current levels, although individual line-specific current values could not be derived from the publicly available data.

Lateral profile measurements

Representative lateral-profile measurements were performed for the HS Link overhead-line section and the AK Link underground-cable section under relatively stable operating conditions. The measurement profiles for the HS Link overhead-line section are shown in Figs 3 and 4, and those for the AK Link underground-cable section are shown in Figs 5 and 6. Figures 3–5 show the profiles measured during bipolar single-circuit operation, whereas Fig. 6 shows the profile measured during monopolar single-circuit operation.

The measured profiles showed a decrease in resultant magnetic flux density with increasing lateral distance from the line or cable route. For the representative overhead-line profiles, the measured values near the direct-current lines diminished to local geomagnetic-field levels at lateral distances of $\sim$40 m from the line centre. For the representative underground-cable profiles, the field was more spatially concentrated near the cable route and diminished to the local geomagnetic-field level within $\sim$20 m. These distances should be interpreted as practical indicators under the investigated conditions, not as general exclusion distances or route-wide limits.

In addition, Figs 5 and 6 indicate that the monopolar single-circuit case showed a field distribution broadly similar to that of the bipolar case under the operating conditions considered here.

Geomagnetic-field-aware calculation for representative profiles

A geomagnetic-field-aware calculation was performed for representative HS and AK profiles for which line-specific current and geometric information were available. The magnetic field calculation was performed using CRIMAG 2010, a power-line magnetic field calculation program based on the Biot–Savart law developed by the Central Research Institute of Electric Power Industry

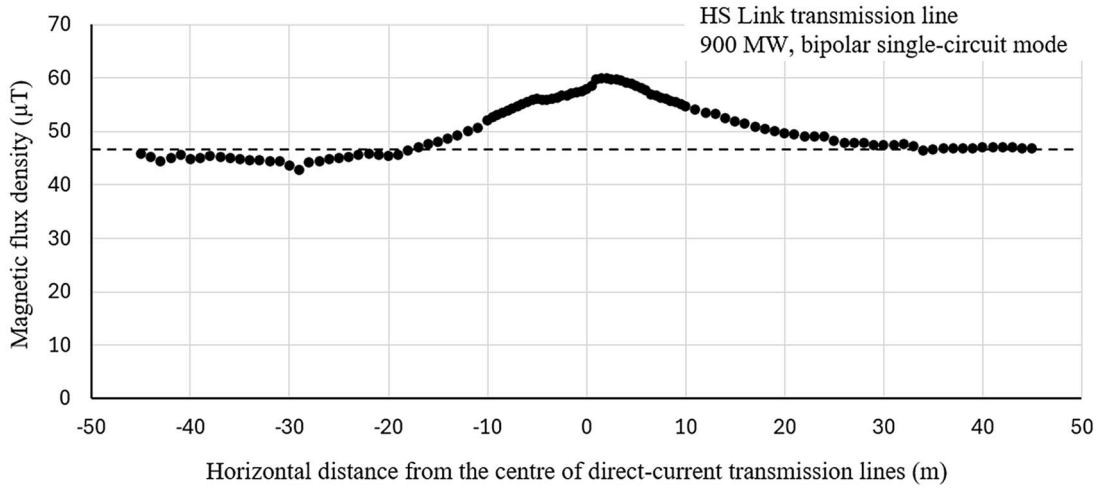


Figure 3 Measured lateral profiles at a height of 1.0 m above ground level for the overhead-line section between towers No. 194 and No. 195 of the HS Link, where measurements were performed on 25 April 2024, when the link was operated in bipolar single-circuit mode with a transmitted power of 900 MW and a current of 2250 A per conductor. Circles indicate measured values, and the dashed line indicates the local geomagnetic-field level. The horizontal distance is measured from the centre of the direct-current transmission line.

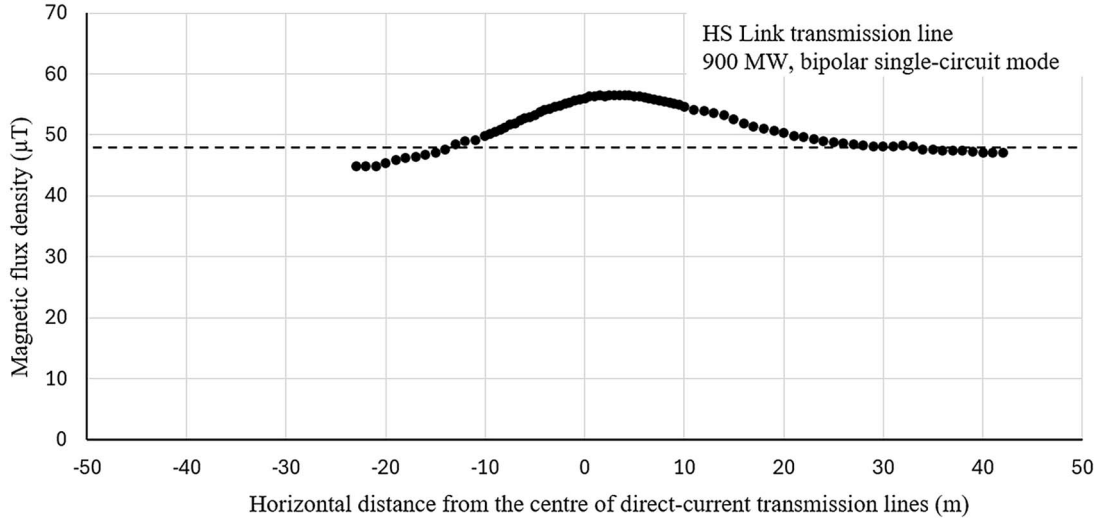


Figure 4 Measured lateral profiles at a height of 1.0 m above ground level for the overhead-line section between towers No. 196 and No. 197 of the HS Link, where measurements were performed on 25 April 2024, when the link was operated in bipolar single-circuit mode with a transmitted power of 900 MW and a current of 2250 A per conductor. Circles indicate measured values, and the dashed line indicates the local geomagnetic-field level. The horizontal distance is measured from the centre of the direct-current transmission line.

[24]. The calculation combined line-generated magnetic-field components with geomagnetic-field components transformed into the line-aligned coordinate system. Details of the calculation procedure, conductor and cable configurations, and measurement–calculation comparisons are provided in the Supplementary Material. Specifically, Supplementary Fig. S1 illustrates the coordinate systems used for the geomagnetic-field transformation. Supplementary Figures S2 and S3 show, respectively, the conductor arrangement and measurement–calculation comparison for the representative HS Link overhead-line profile shown in Fig. 3. Supplementary Figures S4 and S5 provide the corresponding information for the profile shown in Fig. 4, Supplementary Figs S6 and S7 for the profile shown in Fig. 5, and Supplementary Figs S8 and S9 for the profile shown in Fig. 6. The supplementary

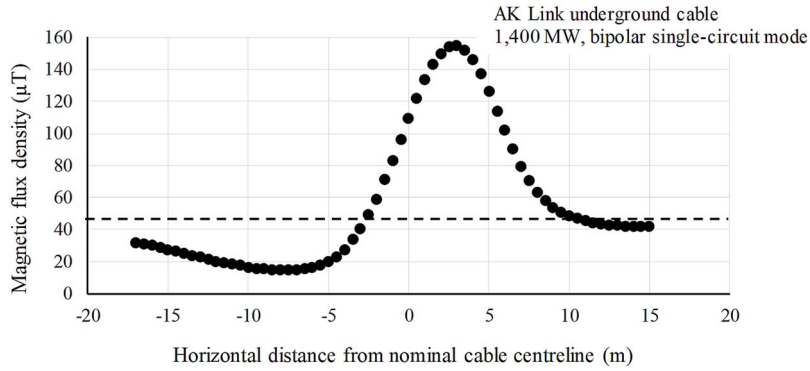


Figure 5 Measured lateral profiles at a height of 1.0 m above ground level for the underground-cable section near the Yura Switching Station of the AK Link, where measurements were performed on 12 December 2023, when the link was operated in bipolar single-circuit mode with a transmitted power of 1400 MW and a current of 2800 A per cable. Circles indicate measured values, and the dashed line indicates the local geomagnetic-field level. The horizontal distance is measured from the nominal cable centreline.

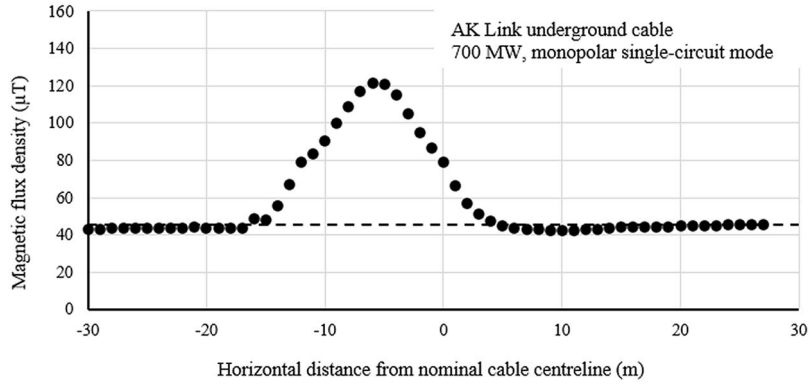


Figure 6 Measured lateral profiles at a height of 1.0 m above ground level for the underground-cable section near the Yura Switching Station of the AK Link, where measurements were performed on 30 May 2024, when the link was operated in monopolar single-circuit mode with a transmitted power of 700 MW and a current of 2800 A per cable. Circles indicate measured values, and the dashed line indicates the local geomagnetic-field level. The horizontal distance is measured from the nominal cable centreline.

comparisons showed good agreement for the representative overhead-line profiles. For the underground-cable profiles, the calculations reproduced the peak magnitudes, although the lateral profile comparison was sensitive to uncertainty in the assumed cable centreline position. These results indicate that the geomagnetic-field-aware calculation procedure can support interpretation of measured lateral profiles when current values and conductor or cable geometry are well defined. These calculations were used together with the measurements to support interpretation of the lateral profiles and to assess the consistency between measured and estimated field levels.

Discussion

This study provides field-measurement data on static magnetic fields around operating direct-current transmission lines in Japan. While previous direct-current magnetic-field studies have mainly focused on marine environments and submarine cables, this study addresses onshore overhead-line and underground-cable sections under actual operating conditions. The results therefore provide reference data directly relevant to on-land environmental monitoring and exposure assessment of static magnetic fields around operating direct-current infrastructure.

Across the measurement locations, the measured resultant static magnetic flux density, including the geomagnetic-field contribution, ranged from 39.7 to 154.8 μT, whereas the local geomagnetic-field levels measured sufficiently far from the transmission lines or cable routes ranged from 46.6 to 50.6 μT. The highest value, 154.8 μT, was observed in an underground-cable section of the AK Link. These results indicate that, under the investigated operating conditions, facility-related static magnetic fields

were measurable near the facilities but remained small in absolute magnitude.

From the viewpoint of radiation protection, the most important finding is the large margin between the measured values and the international reference level for exposure to static magnetic fields. The ICNIRP reference level for general public exposure to static magnetic fields is 400 000 μT [25]. The maximum measured value in this study, 154.8 μT, corresponds to $\sim$0.039% of the ICNIRP reference level. Expressed differently, the maximum measured value was $\sim$2600 times lower than the ICNIRP reference level. Therefore, even at the location where the highest field was observed, the measured static magnetic field was far below the level used for general-public exposure protection.

The differences between overhead-line sections and underground-cable sections can be interpreted mainly in terms of conductor or cable geometry and operating current. In the overhead-line sections, the maximum measured value was 59.9 μT. At many accessible measurement locations, the conductors were relatively high above ground, resulting in a large distance between the conductors and the measurement point. Consequently, the facility-related contribution at ground level was generally small compared with the local geomagnetic-field level. In contrast, measurements in underground-cable sections were conducted above or near the nominal cable routes, where the distance between the sensor and the current-carrying conductors was shorter. This measurement geometry explains why larger local increases were observed in some underground-cable sections.

Among the underground-cable measurements, the highest measured value was observed in the underground-cable section of the AK Link. This result cannot be explained by burial depth alone, because the AK Link was not necessarily the shallowest cable section among the investigated facilities. Rather, the higher values are consistent with the larger operating current of the AK Link during the measurement period. The measured static magnetic flux density near direct-current facilities should therefore be understood as the result of several combined factors, including operating current, conductor or cable arrangement, sensor-to-conductor distance, current polarity, measurement position, and vector superposition with the geomagnetic field.

The lateral-profile measurements provide additional information on the spatial extent of the facility-related static magnetic-field contribution. In the representative overhead-line profiles, the measured resultant magnetic flux density decreased with increasing lateral distance from the line and reached the local geomagnetic-field level at $\sim$40 m from the line centre under the investigated conditions. In the representative underground-cable profiles, the field was more spatially concentrated near the cable route and reached the local geomagnetic-field level within $\sim$20 m of the cable route. These results provide a practical indication of the spatial extent of measurable static magnetic-field influence from the transmission facilities under the investigated operating conditions. Furthermore, the lateral-profile measurements for the underground-cable section of the AK Link showed broadly similar spatial distributions under bipolar and monopolar single-circuit operation, although the peak values differed between the two measurement days. This observation is limited to the investigated AK Link profiles and operating conditions. The broadly similar profile shape can be explained by magnetic-field cancellation effects in both operating modes. During bipolar operation, currents with opposite polarities flow in the main conductors, resulting in partial cancellation of the magnetic field. During monopolar single-circuit operation, currents flowing in opposite directions in the main conductor and the return path similarly produce a magnetic-field cancellation effect comparable to that observed during bipolar operation.

An important feature of static magnetic-field assessment is that the measured quantity is the resultant magnetic flux density, including both the geomagnetic field and the field produced by the direct-current facilities. Because magnetic flux density is a vector quantity, the facility-related field does not simply add as a scalar quantity to the geomagnetic field. Depending on the relative direction of the facility-generated field and the geomagnetic field, the resultant field may increase or decrease locally. This point is particularly important when the facility-related contribution is of the same order as the geomagnetic field.

Measurements and calculations provide complementary information for static magnetic-field assessment around direct-current transmission facilities. Calculations are essential for planning, permitting, and prospective assessment before facilities are constructed, whereas measurements under actual operating conditions provide environmental monitoring data and can be used to confirm the reasonableness of calculation-based estimates. In this study, measured resultant magnetic flux densities were used to characterize field levels under actual operating conditions, while geomagnetic-field-aware calculations were used to examine the consistency between measured and estimated representative lateral profiles and to support their interpretation.

A geomagnetic-field-aware calculation procedure was applied to representative profiles where line-specific current and geometric information were available. The supplementary comparisons showed good agreement for the representative overhead-line profiles. For the underground-cable profiles, the calculations reproduced the peak magnitudes, although the lateral profile comparison was sensitive to uncertainty in the assumed

cable centreline position. These results indicate that the geomagnetic-field-aware calculation procedure can support interpretation of measured lateral profiles when current values and conductor or cable geometry are well defined.

Several factors should be considered when interpreting the measured values. These include instrument accuracy, sensor height and alignment, local magnetic disturbances from nearby metallic objects, temporal variation in operating current and geomagnetic-field estimation. This study was intended to provide environmental monitoring data under actual operating conditions rather than a full metrological uncertainty budget. These factors are not expected to affect the qualitative exposure-assessment conclusion that the measured values at the selected locations and operating conditions were far below the ICNIRP reference level, because the maximum measured value was ∼2600 times lower than the reference level. However, the same factors are relevant when interpreting small differences from local geomagnetic-field levels. These considerations define the interpretation range of the present dataset rather than undermining its value.

Conclusion

This study presented a consolidated on-land dataset of static magnetic fields measured around all operating direct-current transmission links in Japan, including both overhead-line and underground-cable sections under actual operating conditions. Measurements performed at 38 locations showed resultant magnetic flux densities ranging from 39.7 to 154.8 μT, with the highest value observed in the underground-cable section of the AK Link. Even this maximum remained several orders of magnitude below the ICNIRP reference level for general public exposure to static magnetic fields [25].

Representative lateral-profile measurements showed that the resultant magnetic flux density diminished with distance from the line or cable route to local geomagnetic-field levels within several tens of metres under the investigated conditions. These findings provide environmental monitoring data for static magnetic-field exposure assessment around operating direct-current facilities. Geomagnetic-field-aware calculations described in the Supplementary Material were generally consistent with representative measured profiles, although underground-cable comparisons were sensitive to cable-centreline uncertainty.

Acknowledgments

The authors would like to thank Norihiro Minami (currently with Kansai Transmission and Distribution, Inc.) and Yuji Takada (currently with Tohoku Electric Power Network Co., Inc.) for their cooperation in the measurements. The authors also thank Shiina of the Central Research Institute of Electric Power Industry (CRIEPI) for assistance with data analysis.

Author contributions

Fumiaki Kawabe contributed to conceptualization, methodology, investigation, and writing of the original draft. Shinichi Muroya contributed to review and editing and project administration. Chiyoji Ohkubo contributed to supervision. All authors read and approved the final manuscript.

Supplementary information

Supplementary data is available at *Radiation Protection Dosimetry* online.

The Supplementary Material provides details of the geomagnetic-field-aware calculation procedure, coordinate transformation, conductor and cable configurations, measurement–calculation comparisons, and shifted-centreline sensitivity analyses for representative profiles.

Conflict of interests

The authors declare that they have no competing interests.

Funding

This work received no external funding.

Data availability statement

All publicly disclosable measurement results supporting the conclusions of this study are included in the article, particularly in Tables 3 and 4 and in Figs 3–6. Detailed site-specific records, exact measurement coordinates, raw component records, cable-centreline information, engineering drawings, and other infrastructure-related input data are not publicly available because they concern critical electricity transmission infrastructure and/or are subject to restrictions by facility operators. Publicly available data sources used in this study, including power-flow data from OCCTO and geomagnetic-field data from the Geospatial Information Authority of Japan, are cited in the References.

References

1. Organization for Cross-regional Coordination of Transmission Operators, Japan. *Wide-area grid long-term policy. Committee Report.* Tokyo, Japan:

Organization for Cross-regional Coordination of Transmission Operators, Japan, 2023; https://www.occto.or.jp/news/kouikikeitou_chokihoushin_230329_choukihoushin_sakutei.html (accessed 26 May 2026) (in Japanese).
2. Geospatial Information Authority of Japan. *Geomagnetic chart (total intensity) for the epoch 2020.0*. GSI Technical Material B1-No.85. Tsukuba, Japan: Geospatial Information Authority of Japan, 2022.
3. Tsukada T, Kato H, Yomori H. *et al.* Static and ELF magnetic field levels generated by photovoltaic system. In: Annual Conference Committee of the Fundamentals and Materials Society, IEE Japan (ed.). *Proceedings of the IEEJ Fundamentals and Materials Society Conference*. Tokyo, Japan: The Institute of Electrical Engineers of Japan, 2011; VIII-7, 211 (in Japanese).
4. Schmiedchen K, Petri A-K, Driessen S. *et al.* Systematic review of biological effects of exposure to static electric fields. Part II: invertebrates and plants. *Environ Res* 2018;160:60–76. https://doi.org/10.1016/j.envres.2017.09.013.
5. Hermans A, Winter HV, Gill AB. *et al.* Do electromagnetic fields from subsea power cables effect benthic elasmobranch behaviour? A risk-based approach for the Dutch continental shelf. *Environ Pollut* 2024;346:123570. https://doi.org/10.1016/j.envpol.2024.123570.
6. Scott K, Harsanyi P, Easton BAA. *et al.* Exposure to electromagnetic fields (EMF) from submarine power cables can trigger strength-dependent behavioural and physiological responses in edible crab, Cancer pagurus (L.). *J Mar Sci Eng* 2021;9:776. https://doi.org/10.3390/jmse9070776.
7. James E, Ghodsi M, Ford AT. Female crabs are more sensitive to environmentally relevant electromagnetic fields from submarine power cables. *Environ Sci Technol Lett* 2025;12:1487–94. https://doi.org/10.1021/acs.estlett.5c00862.
8. Taormina B, Di Poi C, Agnalt A-L. *et al.* Impact of magnetic fields generated by AC/DC submarine power cables on the behavior of juvenile European lobster (Homarus gammarus). *Aquat Toxicol* 2020;220:105401. https://doi.org/10.1016/j.aquatox.2019.105401.
9. Andrulewicz E, Napierska D, Otremba Z. The environmental effects of the installation and functioning of the submarine SwePol link HVDC transmission line: a case study of the polish marine area of the Baltic Sea. *J Sea Res* 2003;49:337–45. https://doi.org/10.1016/S1385-1101(03)00020-0.
10. Normandeau Associates, Inc., Exponent, Inc, Tricas T, Gill A. *Effects of EMFs from undersea power cables on elasmobranchs and other marine species. OCS Study BOEMRE 2011–09*. U.S. Department of the Interior, Bureau of Ocean Energy Management, Regulation and Enforcement, Pacific OCS Region: Camarillo, CA, 2011.
11. Hutchison ZL, Gill AB, Sigray P. *et al.* Anthropogenic electromagnetic fields (EMF) influence the behaviour of bottom-dwelling marine species. *Sci Rep* 2020;10:4219. https://doi.org/10.1038/s41598-020-60793-x.
12. Sherwood J, Chidgey S, Crockett P. *et al.* Installation and operational effects of a HVDC submarine cable in a continental shelf setting: Bass Strait, Australia. *J Ocean Eng Sci* 2016;1:337–53. https://doi.org/10.1016/j.joes.2016.10.001.
13. Hutchison ZL, Sigray P, He H. *et al. Electromagnetic field (EMF) impacts on elasmobranch (shark, rays, and skates) and American lobster movement and migration from direct current cables*. *OCS Study BOEM 2018–003*. Sterling, VA: U.S. Department of the Interior, Bureau of Ocean Energy Management, 2018.
14. Shiina T, Miyajima K, Sugimoto K. *et al.* Assessment of DC magnetic field under a 200 kV DC overhead transmission line. *IEEJ Trans Power Energy* 2022;142:568–9. https://doi.org/10.1541/ieejpes.142.568.
15. Bracken TD. The HVDC transmission line environment. In: Bracken TD (ed.). *Proceedings of the Workshop on Electrical and Biological Effects Related to HVDC Transmission*. Pacific Northwest Laboratory: Richland, 1979.
16. Takenouchi T, Mizushima K, Kato Y. *et al. Hokkaido-Honshu HVDC link*. Paper 14-03. Paris, France: CIGRE Session, 1980.
17. Nagai T, Mori M, Uchiumi T. *et al. Results of ground fault test and response to actual ground fault of the new Hokkaido-Honshu HVDC Link*. Paper B4-10730_2022. Paris, France: CIGRE Paris Session, 2022.
18. Fujioka S, Takechi M, Harada H. *et al. The construction of the Hida-Shinano HVDC link*. Paper B4-133_2018. Paris, France: CIGRE Paris Session, 2018.
19. Takechi M, Kaneko M, Matsuda T. *et al. System study and commissioning test of the Hida-Shinano HVDC Link*. Paper B4-10731_2022. Paris, France: CIGRE Paris Session, 2022.
20. Shimato T, Hashimoto T, Sampei M. *The Kii Channel HVDC Link in Japan*. Paper 14-106_2002. Paris, France: CIGRE Paris Session, 2002.
21. IEC. *IEC 61786–1:2013. Measurement of DC magnetic, AC magnetic and AC electric fields from 1 Hz to 100 kHz with regard to exposure of human beings—Part 1: Requirements for measuring instruments*. International Electrotechnical Commission: Geneva, 2013.
22. IEC. *IEC 61786–2:2014. Measurement of DC magnetic, AC magnetic and AC electric fields from 1 Hz to 100 kHz with regard to exposure of human beings—Part 2:*

Basic standard for measurements. International Electrotechnical Commission: Geneva, 2014.
23. IEC. *IEC 62110:2009. Electric and magnetic field levels generated by AC power systems—Measurement procedures with regard to public exposure*. International Electrotechnical Commission: Geneva, 2009.
24. Shiina T, Yamazaki K, Ohmura Y. *et al. Establishing reference models for calculation of magnetic fields near electric power facilities*. Paper 5304883. Paris, France: CIGRE 2023 Sendai Colloquium, 2023.
25. International Commission on Non-Ionizing Radiation Protection. Guidelines on limits of exposure to static magnetic fields. *Health Phys* 2009;96:504–14. https://www.icnirp.org/cms/upload/publications/ICNIRPstatgdl.pdf. https://doi.org/10.1097/01.HP.0000343164.27920.4a.

© The Author(s) 2026. Published by Oxford University Press. This is an Open Access article distributed under the terms of the Creative Commons Attribution-NonCommercial License (https://creativecommons.org/licenses/by-nc/4.0/), which permits non-commercial re-use, distribution, and reproduction in any medium, provided the original work is properly cited. For commercial re-use, please contact reprints@oup.com for reprints and translation rights for reprints. All other permissions can be obtained through our RightsLink service via the Permissions link on the article page on our site—for further information please contact journals.permissions@oup.com.
Radiation Protection Dosimetry, 2026, 202, 1552–1564
https://doi.org/10.1093/rpd/ncag089
Paper